


Article

Recycling of Flash-Calcined Dredged Sediment for Concrete 3D Printing

Jana Daher ^{1,2}, Joelle Kleib ^{1,2}, Mahfoud Benzerzour ^{1,2}, Nor-Edine Abriak ^{1,2} and Georges Aouad ^{1,2,3,*} ¹ IMT Nord Europe, Institut Mines-Télécom, Centre for Materials and Processes, F-59000 Lille, France² Univ. Lille, Institut Mines-Télécom, Univ. Artois, Junia, ULR 4515, LGCgE—Laboratoire de Génie Civil et geo Environnement, F-59000 Lille, France³ Faculty of Engineering, University of Balamand—UOB, Qalhat, Lebanon

* Correspondence: georges.aouad@imt-nord-europe.fr; Tel.: +33-327-712-420

Abstract: Due to the large volumes of sediments dredged each year and their classification as waste materials, proper management is needed to efficiently dispose of or recycle them. This study aimed to recycle flash-calcined dredged sediment in the development of an eco-friendly 3D-printable mortar. Mortars with 0, 5, 10, 15, 20, and 30% of flash-calcined sediment were studied. Two tests were carried out to determine the printability of the mixtures. First, a manual gun device was used to examine the extrudability, then a modified minislump test was conducted to assess the buildability and shape-retention ability of the mixtures. Furthermore, the flow table test and the fall cone test were used to evaluate the workability and structural buildup, respectively. The compressive strength was also evaluated at 1, 7, and 28 days for printed and nonprinted mortar specimens. In addition, isothermal calorimetry measurements were conducted on corresponding cement pastes. The results showed that it was possible to print mortars with up to 10% of flash-calcined sediment with the preservation of extrudability and buildability. The results showed that flash-calcined sediment shortened the setting time, decreased the flowability, and enhanced the shape-retention ability. Nonprinted samples with 5% and 10% of flash-calcined sediment showed a similar to higher compressive strength compared to that of the reference mortar. However, printed samples recorded an equal to lower compressive strength than that of nonprinted samples. In addition, no significant change in the hydration process was detected for blended cement pastes compared to the reference cement paste.

Keywords: three-dimensional printing; mortar; recycling; flash-calcined sediment; cementitious material



Citation: Daher, J.; Kleib, J.; Benzerzour, M.; Abriak, N.-E.; Aouad, G. Recycling of Flash-Calcined Dredged Sediment for Concrete 3D Printing. *Buildings* **2022**, *12*, 1400. <https://doi.org/10.3390/buildings12091400>

Academic Editor: Jianguang Fang

Received: 12 August 2022

Accepted: 3 September 2022

Published: 7 September 2022

Publisher's Note: MDPI stays neutral with regard to jurisdictional claims in published maps and institutional affiliations.



Copyright: © 2022 by the authors. Licensee MDPI, Basel, Switzerland. This article is an open access article distributed under the terms and conditions of the Creative Commons Attribution (CC BY) license (<https://creativecommons.org/licenses/by/4.0/>).

1. Introduction

The preservation of natural resources and the recycling of waste materials and by-products in the cement/concrete industry have received much attention lately to maintain a sustainable development, especially with the ongoing release of CO₂ emissions resulting from cement manufacturing. In addition, each year in France, the volume of dredged sediments reaches around 50 Mm³ [1]. There exist already some fields of application where sediments are currently being recycled, such as road and road underlays construction [2] and bricks production [3–6]. Recently, studies have been focusing on reusing sediments as alternative materials in concrete to reduce the environmental impact resulting from cement manufacturing and limit the consumption of natural resources for concrete production [1,7–12]. These studies have shown that incorporating sediments in cement, mortar, and concrete is very promising.

Recently, an innovative and low-energy consumption method called flash calcination has also been applied to efficiently treat sediments by activating certain sedimentary phases, including clay phases [13]. Treatment by flash calcination is classified as a heat treatment where the material in question gets rapidly exposed, within a few seconds, using a technique initially developed by Salvador in 1992 [14], in the presence of air and

under high temperatures. This method aims to create reactive pozzolanic properties in the material in question by activating certain phases. Even though these performances could be attained using the traditional direct calcination technique, the flash calcination approach offers various benefits, including a reduction in energy costs, CO₂ emissions, and calcination time [14,15].

Although many studies have been carried out on the use of dredged sediments in the construction field, to date, there are no studies on their utilization in the field of concrete 3D printing.

Three-dimensional printing is an additive manufacturing (AM) process that assembles materials to manufacture objects from 3D models, generally, layer after layer as defined by ASTM [16]. Therefore, AM is an automated process that produces 3D-printed objects in consecutive layers using computer-aided design (CAD). It was first introduced in the 1980s [17] and has received more and more attention in recent years. It spread rapidly through the years for several types of materials such as metals [18], ceramics [19], and polymers [20], towards several fields of application such as the aircraft industry [21], medical instruments [22], and the food industry [23]. In 1997, cementitious materials were firstly introduced in AM [24]. Currently, there are three main types of AM of cementitious materials used in construction/architectural applications: contour crafting [25], D-Shape [26], and concrete printing [27,28]. In addition, AM or 3D printing presents many advantages over the conventional construction method by allowing multiscale architectural complexity/flexibility, reducing labor, construction costs, the use of molds, and construction time.

For a mortar to be considered printable, several specifications must be met. According to Le et al. [29] and Tay et al. [30], workability, extrudability, buildability, and open time act as essential parameters to qualify the material used. First, the material must be workable and fluid enough to exit the printer nozzle without causing blockage or segregation. This behavior—related to the initial workability and viscosity of the material—is called extrudability [29,30]. Then, once the material gets extruded, and for the possibility to superpose layers, the printed filaments must hold their proper weight and the load of all deposited layers above at a very early age to ensure stability and prevent failure of the printed structure [29,30]. This behavior, which relates to the open time and the material's yield stress, is called "buildability" [27,31].

However, it is largely known that in order to fulfill the necessary requirements (extrudability and buildability) for 3D-printing materials used in construction, most printable cementitious mixtures contain large cement content, which is associated with high costs, high CO₂ emissions, and a negative environmental impact [32]. For this reason, in the past few years, studies have been mainly focusing on reducing costs, environmental impact, CO₂ emissions, and high cement contents in concrete 3D printing, by implementing supplementary cementitious materials [29,33–36], using low-impact admixtures [37,38] and recycling industrial waste materials [39,40]. For example, Rehman et al. [41] tried incorporating municipal solid waste incineration fly ash and bottom ash in concrete 3D printing. The addition of fly ash increased the setting time and enhanced the initial yield stress of printed materials, allowing a rapid construction speed with concrete 3D printing. Ilcan et al. [42] investigated the rheological properties and compressive strength of geopolymer mortars based on construction and demolition waste for 3D printing. Ding et al. [43] studied the early age mechanical behavior of 3D cement mortar using recycled sand.

This study aims to recycle dredged sediment in the development of an environmentally friendly 3D-printable mortar. Thus, thermally treated flash-calcined sediment was used as a partial substitute for cement to help promote a printable mortar that reduced cement consumption while enabling waste material valorization. Hence, to meet these requirements, all of the developed mortars in this study were characterized in both fresh and hardened states. Several parameters were examined and evaluated, such as workability, printability (extrudability and buildability) at laboratory and gantry printer scales, structural buildup and yield stress evolution with respect to time, and hardened properties such as compressive strength.

2. Materials and Methods

2.1. Materials

The materials used in this study are ordinary Portland cement (OPC), CEM I 52.5N, provided by EQIOM (France), fluvial sediment (FS) from Noyelles-sous-Lens (France) thermally treated by the method of flash calcination at 750 °C, and a 0/2 mm crushed calcareous sand provided by Carrières du Boulonnais (France) having a density of 2.74 g/cm³. The density, the median particle diameter (D50), and the specific surface area (BET) of cement and flash-calcined sediment are presented in Table 1. In addition, two admixtures provided by CHRYSO were used: CHRYSO® Fluid Optima 100 as a superplasticizer/high range water reducer (HRWR) having a dry content of 31% ± 1.5% and BELITEX® ADDICHAP as a viscosity modifying agent (VMA) in the form of a white powder.

Table 1. Density, median particle diameter, and specific surface area of cement and flash-calcined sediment.

Powder	Density (g/cm ³)	D50 (μm)	BET (m ² /g)
OPC	3.15	8.82	0.98
FS	2.64	7.22	28.95

The cement and flash-calcined sediment's particle size distribution (PSD) was measured using an LS 13 320 laser diffraction particle size analyzer and is shown in Figure 1. The particle size of the sediment is close to that of the cement, which makes the substitution of cement by sediment possible and promising.

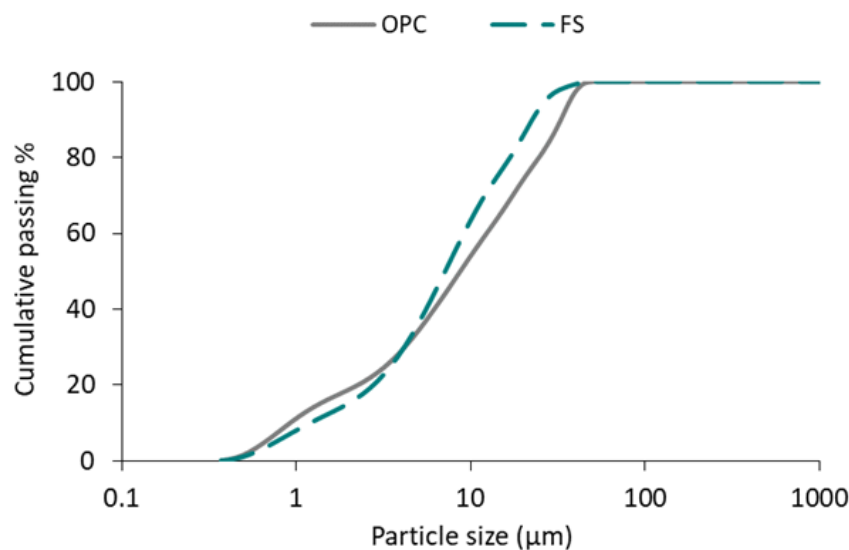


Figure 1. Particle size distribution of cement and flash-calcined sediment.

2.2. Mix Design

All components and their proportions have to be carefully determined to achieve the desired quality and performance of a printable mixture. Thus, in this study, in order to evaluate the effect of replacing OPC with flash-calcined sediment on the properties of a printable mortar, mixtures with different substitution percentages (5, 10, 15, 20, and 30%) were studied. A reference mixture with 0% substitution was also defined and characterized to better understand the behavioral changes in mortar properties attributed to the addition of flash-calcined sediment. All substitutions were done by volume. The water/binder ratio (W/B) and the admixtures concentrations were kept constant to uniquely study the effect of increased sediment content on the fresh and hardened properties of the mixtures. Therefore, the W/B ratio was kept at 0.4, whereas the VMA and the liquid HRWR concentrations

were set at 0.4% and 0.8% of the binder's weight, respectively. The mix design of tested mortars is presented in Table 2, where REF corresponds to the reference mixture with 0% sediment added, and the others correspond to the mixtures with sediment addition (i.e., FS10 corresponds to the mixture with 10% of added flash-calcined sediment).

Table 2. Mix design of tested mortars.

Mixtures	REF	FS5	FS10	FS15	FS20	FS30
Sand (g)	850	850	850	850	850	850
OPC(g)	682.75	648.61	614.48	580.34	546.2	477.93
FS (g)	0	28.61	57	85.83	114.01	171.66
W/B	0.4	0.4	0.4	0.4	0.4	0.4
VMA (%)	0.4	0.4	0.4	0.4	0.4	0.4
HRWR (%)	0.8	0.8	0.8	0.8	0.8	0.8

2.3. Mixing Procedure

The laboratory-scale mixing procedure was performed using a Hobart N50CE mixer with a total mixing duration of 7 min distributed as follows:

- Dry mixing at low speed for all solid ingredients for 2 min;
- Adding water and HRWR for 30 s at low speed;
- Mixing at low speed for 30 additional seconds;
- Mixing at high speed for 1 min;
- Scraping the mixer bowl followed by resting for 1 min;
- Mixing at high speed for 2 min.

2.4. Fresh State Characterization of Mortars

2.4.1. Printability Tests

The printability of the mixtures was first examined at laboratory scale. First, the extrudability of mixtures was assessed using a manual gun device having a 2 cm circular nozzle diameter similar to what was previously used and tested by Khalil et al. [44] and Baz et al. [45]. The tested mixtures were considered extrudable if no problems of blockage or segregation occurred at the level of the nozzle of the gun device during the extrusion process. Then, the buildability and shape-retention ability of mixtures were assessed using a modified minislump test, similarly to what was carried out by Nematollahi et al. [46] and Ilcan et al. [42]. The test consisted of filling freshly mixed mortar into the minislump cone having an initial height of 5 cm, lifting the cone slowly, and placing a static load of 600 g on the top surface of the cone-shaped mortar (including the weight of a round glass plate), then measuring the final average height of the deformed fresh specimen after 1 min of loading. The higher the final measured height after loading, the higher the shape-retention ability of the mixture. The test setup is shown in Figure 2.

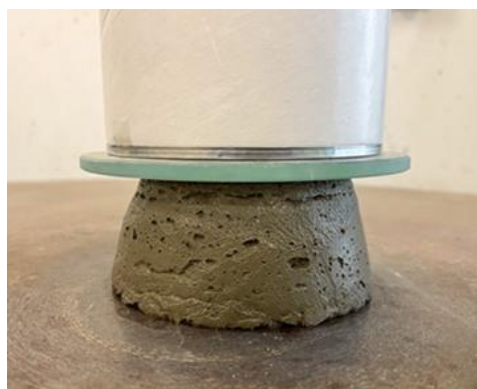


Figure 2. The modified minislump shape-retention ability test.

The printability (extrudability and buildability) was then confirmed on a larger scale using a 3-axis gantry printer, shown in Figure 3, having a similar 2 cm circular nozzle diameter as the gun device.



Figure 3. The 3-axis gantry printer used in this study.

2.4.2. Flow Table Test and Setting Time

The flow table test was used to determine the mortars' flowability and flow diameter following the NF EN 1015-3 standard. In addition, the setting times of the mortars were determined using the Vicat test following the NF EN 480-2 standard. A needle of a diameter equal to $\varnothing = 1.13$ mm was released automatically through the mold containing the specimen every 10 min; then, the distance separating the base of the mold and the bottom of the needle was recorded.

2.4.3. Fall Cone Test

The fall cone test was used in this study to assess the structural buildup and the thixotropic behavior of the tested mortars and was carried out following the European standard NF EN ISO 17892-6 and a study conducted by Baz et al. [47]. Through this test, yield stress values corresponding to a series of recorded penetration depths due to an imposed load of a well-defined cone into the mortars can be calculated using a specific equation [48]. The used cone had an angle of 30° (θ) and a total mass of 230 g. The same procedure and methodology used in the study of Baz et al. [47] were followed in this study, where the penetration depth of the cone into the mixed material placed in a circular steel container was measured each 150 s (2.5 min) for a total duration of 1320 s (22 min). The yield stresses τ in kPa were calculated as shown in Equation (1), where F is the force generated by the cone mass, h is the recorded penetration depth, and θ is the angle of the cone.

$$\tau = F \cos \theta^2 / \pi h^2 \tan \theta \quad (1)$$

2.5. Mechanical Performance of Mortars

The compressive strength of the prepared mortars was assessed to evaluate their mechanical performance. Two methods of mortar placement within molds were adopted. The first method was done according to the European standard placing method NF EN 196-1 on traditional $4 \times 4 \times 16$ cm beams. The second method was done by printing

successive layers inside $4 \times 4 \times 16$ cm prismatic beams. Therefore, in order to achieve a width of 4 cm of printed filaments, a 3×1 cm nozzle was used alongside the same manual gun device used for the extrudability test to print the mortar directly into the $4 \times 4 \times 16$ cm mold in the form of 4 successive layers, similarly to what was conducted in a study by Khalil et al. [44].

Once molded, the specimens were placed at $20\text{ }^{\circ}\text{C}$ and 100% RH, demolded after 24 h, and then cured under the same conditions until the testing dates.

The compressive strength tests of the specimens, regardless of the molding method, were carried out at 1, 7, and 28 days according to the test method of European standard NF EN 196-1. Regarding the direction of testing, the loading force was applied along the flat side surfaces of the specimens, therefore parallel to the printed layers in the case of printed samples (Figure 4). The values obtained from the standard molded samples helped study the effect of the binder composition on the mechanical strength of the mixtures. In contrast, those obtained from the printed specimens allowed us to evaluate the impact of the printing process on the mechanical properties of the blends.

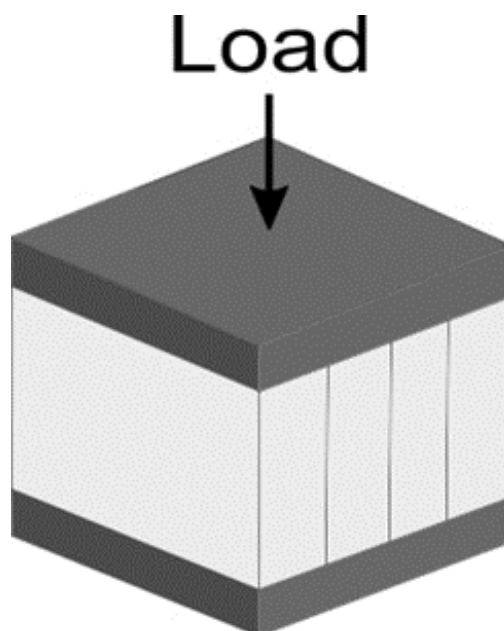


Figure 4. Loading direction force for 3D-printed samples.

2.6. Isothermal Calorimetry Measurements

The characterization of cement pastes was also considered in this study in order to better understand the behavior of blended cement–sediment pastes in printable mortars. The composition of the tested pastes was identical to that of the mortars presented earlier in Table 2, excluding the inclusion of sand. The heat of hydration and the reactivity of the pastes were measured using an isothermal calorimetry test at $20\text{ }^{\circ}\text{C}$ with fluxmeters that allowed the homemade calorimeter to be equilibrated in less than 5 min [49,50]. It is also worth noting that the materials were stored prior to testing in the same isothermal calorimetry testing room at $20\text{ }^{\circ}\text{C}$ to ensure a consistent temperature throughout all phases of testing.

3. Results and Discussion

3.1. Fresh-State Characterization of Mortars

3.1.1. Printability Tests

The extrudability of the mixtures was evaluated using a manual gun device having a circular nozzle diameter of 2 cm. The mixtures were considered extrudable if no problems of blockage or segregation occurred at the gun's nozzle during the extrusion process.

Once extruded, the mixtures were then tested for visual buildability and were considered buildable when the deposited layers held their proper weight and the weight of the layers deposited above them without showing any signs of collapse or failure of the printed element. However, in order to quantitatively assess the buildability and the shape-retention ability of the mixtures, the modified minislump test was carried out and the final height of each of the freshly mixed mortars was measured after deformation due to the added static load of 600 g. The tested mixtures were judged buildable if their final measured height after loading did not fall below 4.5 cm. This value served as the limiting threshold height value for this buildability test and was established utilizing the modified minislump test using a commercial printable mortar.

The extrudability results are shown in Figure 5. On the one hand, REF, FS5, and FS10 were easily extrudable without clogging the nozzle of the manual gun device. On the other hand, FS15 and FS20 were dry and difficult to extrude, had a lot of cracks, and thus could not be printed correctly. Consequently, the addition of flash-calcined sediment resulted in drier, stiffer, and more difficult to extrude mixtures. This behavior could be attributed to the nature of sediments and their high water demand. Moreover, FS30 is not shown in Figure 5 because it was very dry and not at all extrudable. As a result, it was decided to drop FS30 for the rest of the study because the remaining tests could not be performed on that mixture.

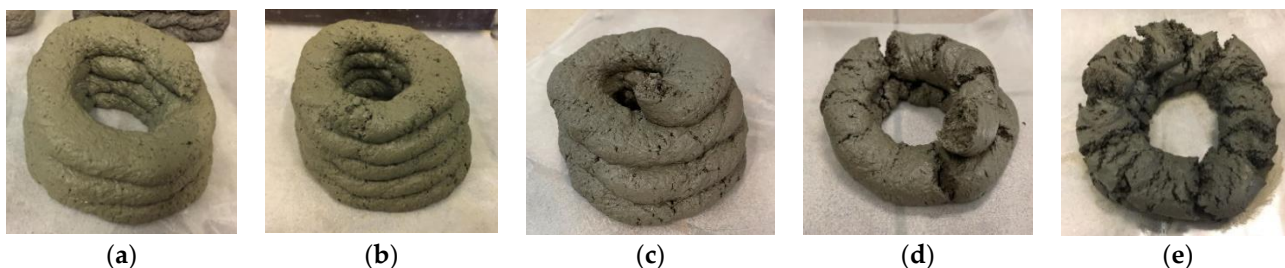


Figure 5. Printing using the manual gun device of (a) REF; (b) FS5; (c) FS10; (d) FS20; and (e) FS30.

The buildability results are shown in Figure 6, where the final measured heights of the different freshly prepared mixtures after deformation due to a static 600 g loading, including that of a commercial 3D-printable mortar, are presented. The results show that all mixtures (REF and blended mortars) had final heights greater than the limiting threshold height value (4.5 cm) with values ranging from 4.5 cm to 4.75 cm. This demonstrates that all mixtures were buildable and had good shape-retention ability.

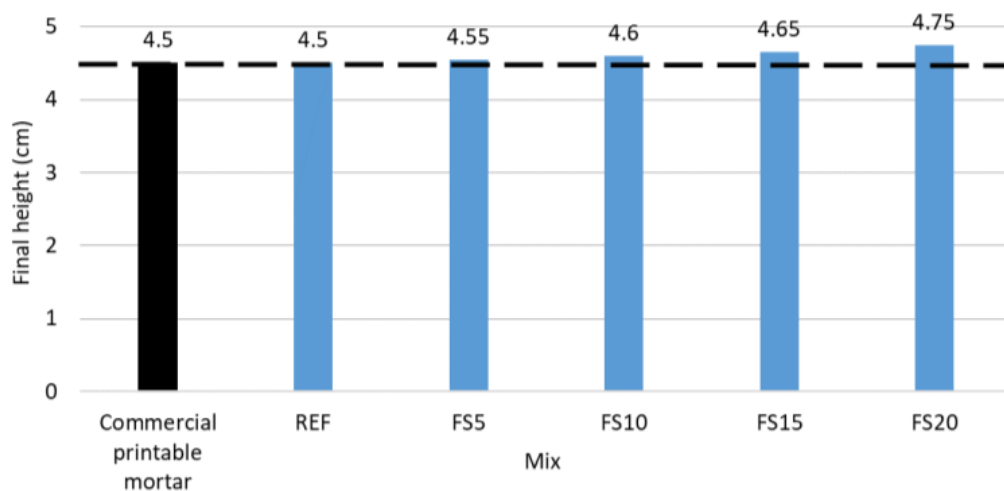


Figure 6. Buildability of mixtures using the modified minislump test.

Furthermore, when comparing the different tested mixtures of this study with each other, it could be seen that the final measured height was higher for mixtures containing greater quantities of flash-calcined sediment. This meant that the addition of flash-calcined sediment led to stiffer and high-shape-retention-ability mixtures. However, not all buildable mixtures could be considered printable, since it was proven earlier in Figure 5 that FS15 and FS20 were not extrudable. Nevertheless, REF, FS5, and FS10 were proven to be printable as well as extrudable, therefore they were considered printable mixtures.

Both manual gun printing test and modified mini-slump test showed that the optimal acceptable amount of flash-calcined sediment that could be added to the mixture while maintaining acceptable extrudability and ensuring sufficient buildability was of 10%. For this reason, FS10 was tested for printability on a larger scale using the gantry printer, as shown in Figure 7.



Figure 7. FS10 mixture printed using the gantry printer.

3.1.2. Flow Table Test and Setting Time

The changes in flow table test results with the addition of flash-calcined sediment are shown in Figure 8 and the mortars' initial and final setting times in Figure 9. Concerning the flow table test results, the workability of the mortars decreased with sediment addition, where REF recorded a flow diameter of 15.59 cm, whereas FS20, for example, recorded a value of 12.59 cm. Similarly, a loss in workability was reported in other studies conducted by Zhao et al. [1] and Rehman et al. [41], where flow diameters of mixtures decreased with the addition of sediment [1] and MSW incineration ash [41]. Here, the loss of workability could be attributed to sediment having a higher specific surface area than cement, which resulted in the absorption of a portion of the mixing water. In addition, the good correlation factor ($R^2 = 0.98$) corresponding to the best fit curve in Figure 8 shows that the decrease in workability is linear with the addition of sediment. Furthermore, it can be seen from Figure 9 that the initial and final setting times of mortars are attained faster with the addition of flash-calcined sediment. It is important to note that setting time can be influenced by several factors including the W/B ratio, the temperature of the mixture, the mineralogical composition, and the presence of admixtures [51]. When referring to Figure 5, and from a visual inspection of the change in fresh state behavior of printed blended mortars, it was predicted that higher sediment contents would result in a faster setting of mortars due to the stiffness and hardness of the mixtures. This behavior, similar to what was obtained in the flowability test, can also be attributed to the high water demand of sediments.

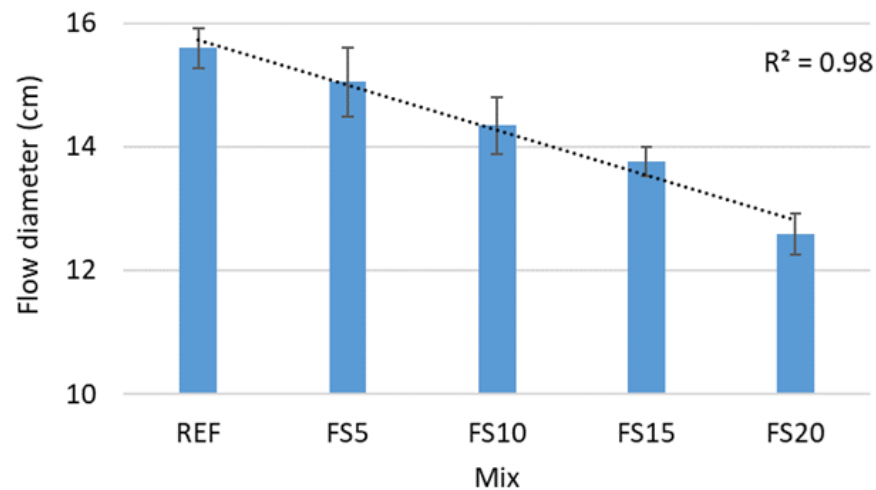


Figure 8. Variation of flow diameter with the addition of flash-calcined sediment.

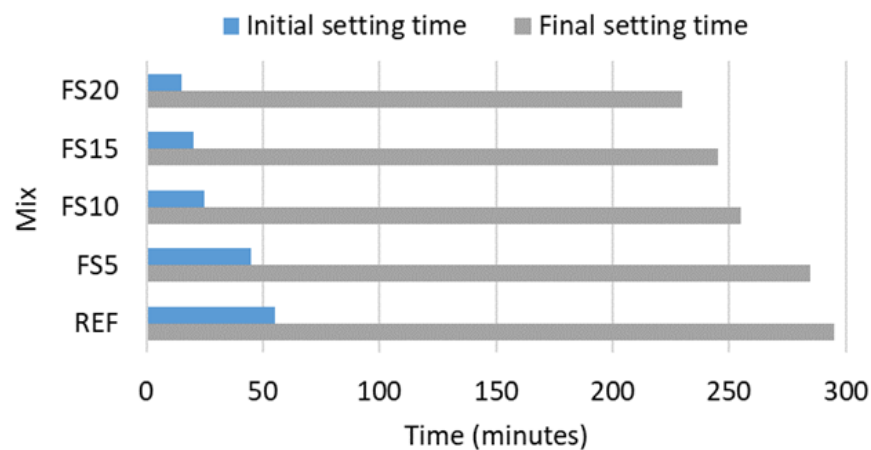


Figure 9. Initial and final setting times of mortars.

The findings of the flow table and setting time tests could help identify some boundary limits of what was discovered with the printability tests in the previous section. Printable mixtures showed a flow diameter larger than 14 cm (i.e., REF, FS5, and FS10), whereas highly stiff nonprintable mixtures recorded a flow diameter lower than 14 cm (i.e., FS15 and FS20). In addition, printable mixtures recorded initial setting times ranging between 25 and 55 min (i.e., REF, FS5, and FS10), whereas nonprintable ones recorded shorter setting times of 15 and 20 min (i.e., FS15 and FS20).

3.1.3. Fall Cone Test

Several researchers have developed methods to estimate and evaluate rheological properties and parameters of printed cementitious materials, such as yield stress, viscosity, thixotropy, and structural buildup. The Bingham model is the most frequently applied viscosity model representing a linear relationship between the equilibrium shear stress and the shear rate. The equilibrium shear stress is obtained by applying a constant shear rate [52]. According to Roussel [53,54], the evolution of the yield stress of printed cementitious materials is linear with time, whereas according to Perrot et al., the development of the yield stress with time starts linear but ends up exponential [31]. Lootens et al. [55] showed that the yield stress could be derived from measuring the penetration with a cylindrical piston of radius R . According to another study by Rahul et al. [56], extrudability and constructability could only be obtained when the yield stress of the printed material was

between 1.5 and 2.5 kPa, while according to Le et al. [29], the optimum value of the yield stress for 3D concrete printing was 0.55 kPa.

Figure 10 shows the fall cone test setup, while Figure 11 shows the variation of the yield stress with the evolution of time for the tested mortars with different sediment additions. The results show that the yield stress increases with time for all mortars. Furthermore, as the sediment content increases, the slope of the curves rises, indicating an increase in the structural buildup of the mortars, which is attributable to the addition of sediment.



Figure 10. Fall cone test setup.

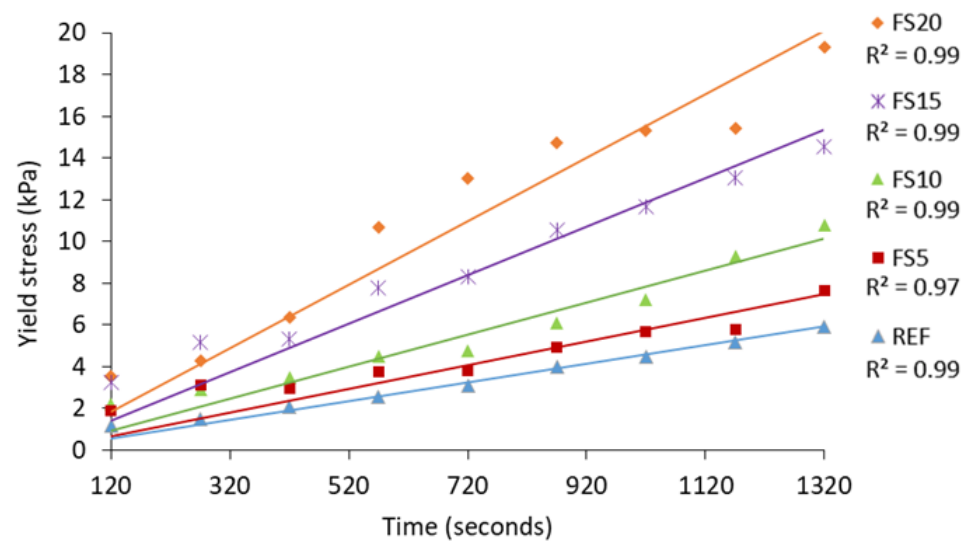


Figure 11. Yield stress evolution of mortars with time.

Comparing the results of this study with those obtained by Baz et al. [47] using the same method, the variation of the yield stress with time could similarly be predicted using a linear model where all mortars' best-fit curves recorded good correlation factor (R^2) ranging between 0.97 and 0.99. This pattern also complied with that of Roussel [53,54], where the evolution of the yield stress of printed cementitious materials was defined to be linear with time. Furthermore, the yield stress values recorded by REF, FS5, and FS10 were close to each other, whereas those recorded by FS15 and FS20 were further apart from the three first mixtures. For the three printable mixtures (REF, FS5, and FS10), the first yield stress recorded at 120 s ranged between 1.2 and 2.2 kPa, which coincided with the findings of the study conducted by Rahul et al. [56], whereas, for FS15 and FS20, the first recorded yield stress was 3.2–3.5 kPa, indicating that the mixtures were too stiff to be printed.

3.2. Mechanical Performance of Mortars

The compressive strength of all mortars was tested using the European standard method NF EN 196-1 on conventionally cast $4 \times 4 \times 16$ cm (nonprinted) beams. However, only REF, FS5, and FS10 were tested for compressive strength on 3D-printed beams made by four consecutive extruded layers of 1 cm height each. FS15 and FS20 mixtures were not evaluated for compressive strength by the second approach since they were not printable, making it impossible to extrude and deposit consecutive layers to form prismatic beams.

The compressive strength results of nonprinted mortars at 1, 7, and 28 days are presented in Figure 12. FS5 and FS10 recorded comparable compressive strength to REF. For example, a modest increase in compressive strength compared to REF was recorded for FS5 at 1 day and for FS5 and FS10 at 28 days. However, the compressive strength slightly decreased for higher substitution rates (FS15 and FS20). This demonstrates that up to 10% addition of flash-calcined sediment can improve the overall resistance by promoting cement hydration development. Similar results were obtained by Amar et al. [57], where the compressive strength of mortars with different W/B ratios (0.4, 0.5, 0.6, 0.7, and 0.8) and different sediment substitution rates (0, 5, 8, 10, 15, 20, and 25%) was tested. They found that the optimum substitution rate of sediment was around 10–15% and that the higher the W/B ratio, the lower the compressive strength of the mortars. They also found that mortars with 5% of sediment addition showed the highest resistance, whereas mortars with 8% and 10% of sediment addition showed similar to higher resistances compared to the reference mixture at 28 days.

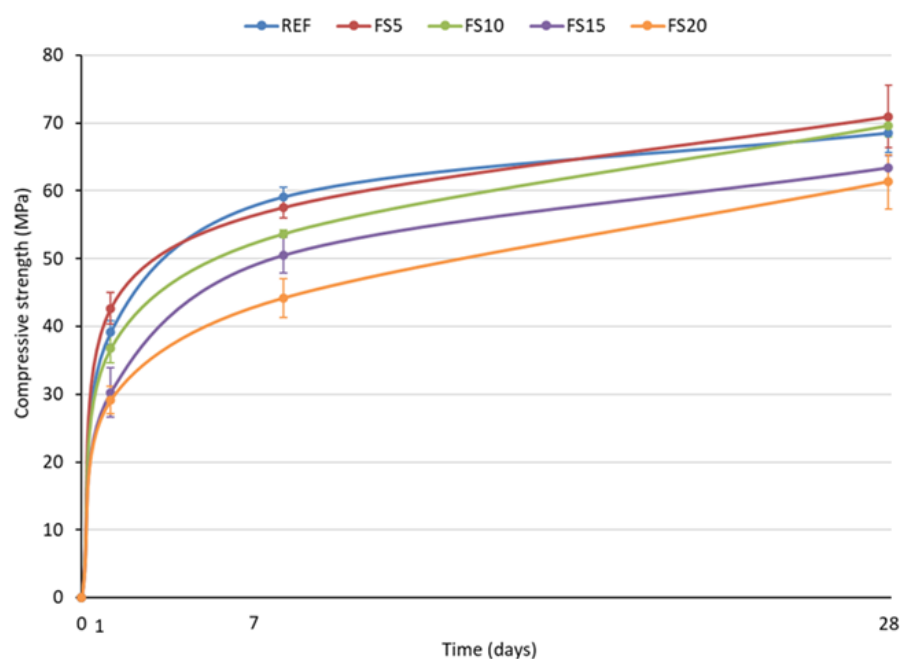


Figure 12. Compressive strength of nonprinted mortars at 1, 7, and 28 days.

In addition, the compressive strength results of nonprinted and printed mortars at 1, 7, and 28 days are presented in Figure 13. At 1 day, a lower compressive strength was recorded for printed samples. Then, at 7 days, an identical compressive strength was recorded for printed and nonprinted mortars. Finally, at 28 days, printed REF and FS5 recorded similar compressive strengths compared to their corresponding nonprinted samples, whereas printed FS10 recorded a significantly lower strength value compared to its nonprinted sample. The low compressive strength in printed samples compared to conventionally cast samples can most likely be due to the greater porosity associated with the placement method, as printed samples are laid down layer by layer without any form of compaction, whereas nonprinted samples are compacted during placement, hence eliminating the higher porosity. Several previous studies have reported a similar behavior when comparing 3D-printed to conventionally cast elements [58,59].

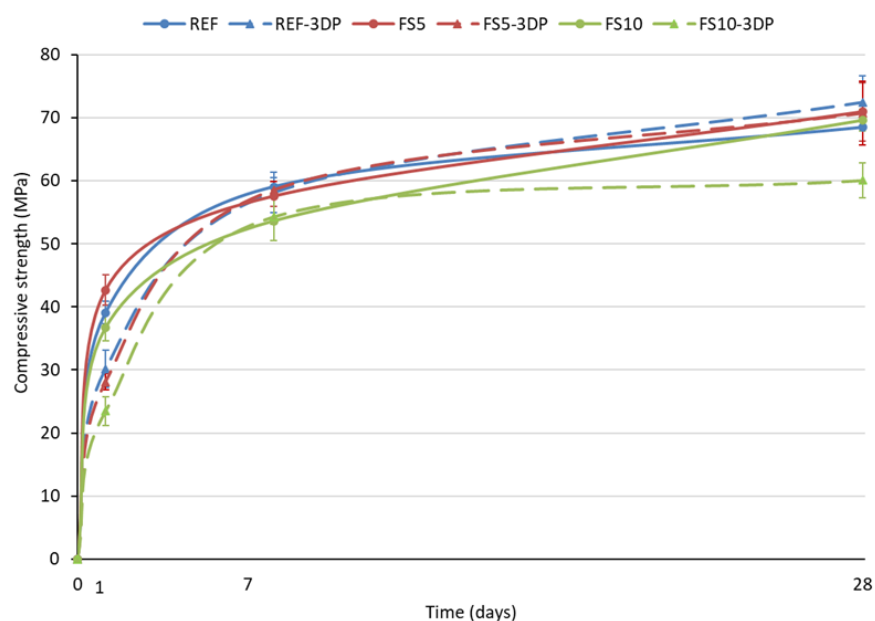


Figure 13. Compressive strength of nonprinted and printed mortars at 1, 7, and 28 days.

Furthermore, by comparing printed samples, REF-3DP and FS5-3DP had compressive strengths that were very close to each other, whereas FS10-3DP recorded lower strength values than both mixtures at all dates, especially at 28 days. This decrease in strength can be associated with the loss of workability resulting from the addition of flash-calcined sediment which is a very fine material that increases the stiffness of the mixture due to its high water demand [1]. Consequently, the mixture containing 10% of flash-calcined sediment was slightly harder to extrude and more challenging to lay in the prismatic mold compared to the REF and FS5 mixtures, creating larger pores and decreasing the compressive strength. However, mixtures with a higher workability (REF-3DP and FS5-3DP) had a better adhesion between printed layers and a lower void formation and therefore did not have as many losses in compressive strength as mixtures with a lower workability.

The stiffness and viscosity of blended mortars can be attributed to the clay content and the fineness of the flash-calcined sediment. Several studies reported similar results when adding nanoclay for example. It was shown that nanoclay affects the fresh and rheological behavior of 3D-printable cementitious materials by playing the role of a natural viscosity-modifying agent [37,38]. Kaushik et al. [38] showed that although adding nanoclay to the cementitious mixture for 3D-printed concrete resulted in a significant loss of workability, the material's yield stress increased due to the mix's higher cohesiveness. The addition of nanoclay helped with the preservation of the ideal shape of the material during and after extrusion, preventing it from collapsing. The addition of sediments in this

study seemed to have similar effects on the fresh and rheological properties of 3D-printed cementitious materials.

Furthermore, it is important to keep in mind that the tested printed beams in this study were developed using a manual gun device that was human-operated, implying that manipulation errors could occasionally occur and affect the mechanical performance of the printed samples.

To look further into the low compressive strength of FS10-3DP at 28 days, which can be due to either the high stiffness/porosity of the mixture or to a human manipulation error using the manual gun device, the compressive strength at 28 days was assessed on samples printed by the gantry printer. Two mixtures were tested: REF-Printer and FS10-Printer. The compressive strength of REF-Printer (gantry printer) and REF-3DP (manual gun device) was 72.83 MPa and 72.51 MPa 3DP, respectively. The results showed that the method of printing did not affect the compressive strength of the REF mixture. However, for FS10, a change in compressive strength was detected with the different printing methods. The result of FS10-Printer (65.19 MPa) was higher than that of FS10-3DP (60.08 MPa), confirming the potential human error for stiff mixes. However, the strength of FS10-Printer at 28 days (similarly to the manual gun result) was still lower than that of REF-Printer, which was not the case in nonprinted samples (Figure 12). For this reason, the total porosity of printed REF-Printer and FS10-Printer was measured at 28 days using mercury intrusion porosimetry (MIP) and is shown in Table 3 as well as their compressive strength. The REF-Printer sample had a total porosity of 10.06% and the FS10-Printer sample of 12.73%. This complied with the compressive strength results of the samples and proved that the low compressive strength of FS10-Printer was due to its high porosity content compared to the REF-Printer. This also confirmed that the addition of flash-calcined sediment did not affect the compressive strength of nonprinted samples since they were compacted and did not contain a high porosity; however, it affected the compressive strength of printed (noncompacted) samples where high voids were still entrapped in the printed sample, consequently reducing the compressive strength.

Table 3. Compressive strength and total porosity of REF-printed and FS10-printed by the gantry printer at 28 days.

Mixtures	Compressive Strength at 28 Days	Total Porosity at 28 Days
REF-Printer	72.83 MPa	10.06%
FS10-Printer	65.19 MPa	12.73%

3.3. Isothermal Calorimetry Measurements

Figure 14 shows the heat and cumulative heat release measured using an isothermal calorimeter for the cement pastes. All the calorimetric heat release curves show similar shapes and tendencies within the first 48 h of the hydration process.

The first phase occurs directly after the contact of water with cement and is related to the dissolution of the anhydrous grains, hence the hydration of cement grains. This phase usually happens very quickly, within a few minutes, and generates a lot of heat [60]. The second phase corresponds to the induction period where cement pastes exhibit a low thermal activity and heat release [61]. The third phase corresponds to the accelerated hydration of silicates and aluminates, forming C-S-H and ettringite, causing a high heat release. Here, the paste begins to set. Lastly, the fourth and final phase is formed after the depletion of gypsum and the transition of ettringite to monosulfoaluminate hydrate, slowing down the reactions, decreasing the heat released, and forming the solid paste matrix [62].

Figure 14 illustrates that all pastes have the same hydration mechanism. They show equal induction period segments and no significant difference or delay in the start of the accelerated hydration stage, which occurs nearly 10 h after the beginning of the hydration process. In addition, the pastes exhibit similar second peak shapes after the induction

phase, with that of the REF paste being the most intense because it contains the most cement compared to the other pastes. This shows that the addition of flash-calcined sediment does not majorly affect the hydration process or the start of the setting of the pastes. Other studies have also proved that the addition of flash-calcined sediment does not negatively affect the cement hydration process [15].

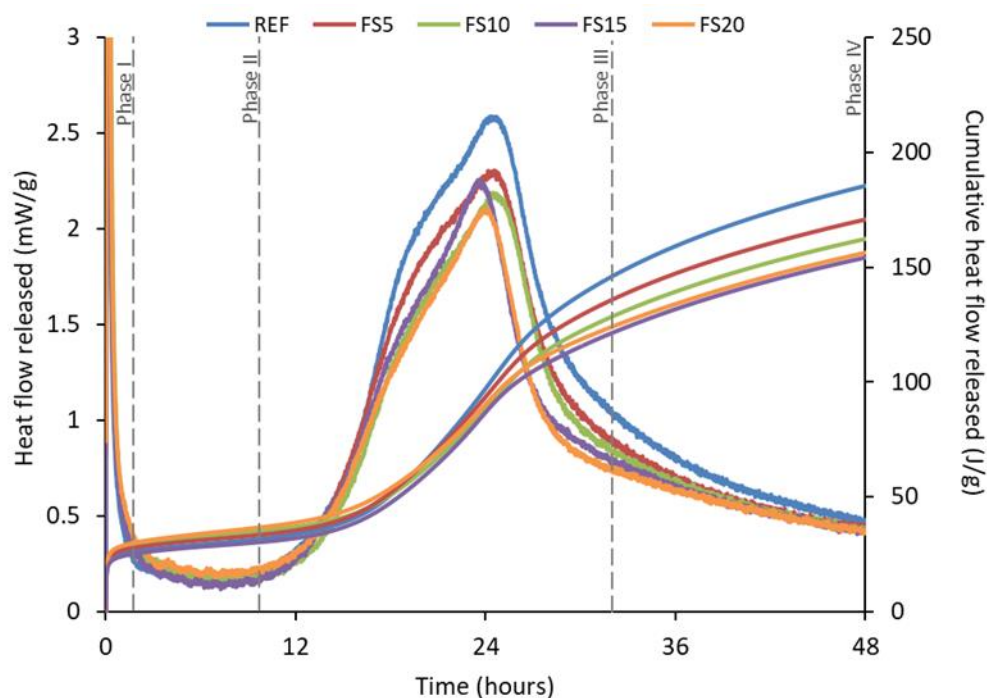


Figure 14. Heat and cumulative heat release of pastes.

Furthermore, within the first 48 h of hydration, the cumulative heat release of the pastes appears to decrease with the increase of sediment addition which is expected due to the effect of cement dilution, especially in the short term. However, flash-calcined sediment was proven to possess a significant pozzolanic reactivity in the longer term [15,57].

Furthermore, Figure 15 illustrates the cumulative heat flow released during the first 60 min of hydration for the REF, FS5, and FS10 pastes, corresponding to the printable REF, FS5, and FS10 mortars, since it is very crucial to monitor the hardening behavior of printable mortars as well as their setting time at a very early age, especially during the first hour of the printing process. The results show that FS10 has the highest cumulative heat of hydration during the first hour, followed by FS5, then REF. Consequently, the addition of flash-calcined sediment led to an increase in the heat of hydration of pastes within the first hour, leading to an accelerated setting time of mortars containing flash-calcined sediment within the first hour of printing. It can therefore be concluded that the results of isothermal calorimetry complied with the results obtained by the Vicat test, where FS10 showed the shortest initial setting time, followed by FS5, then REF.

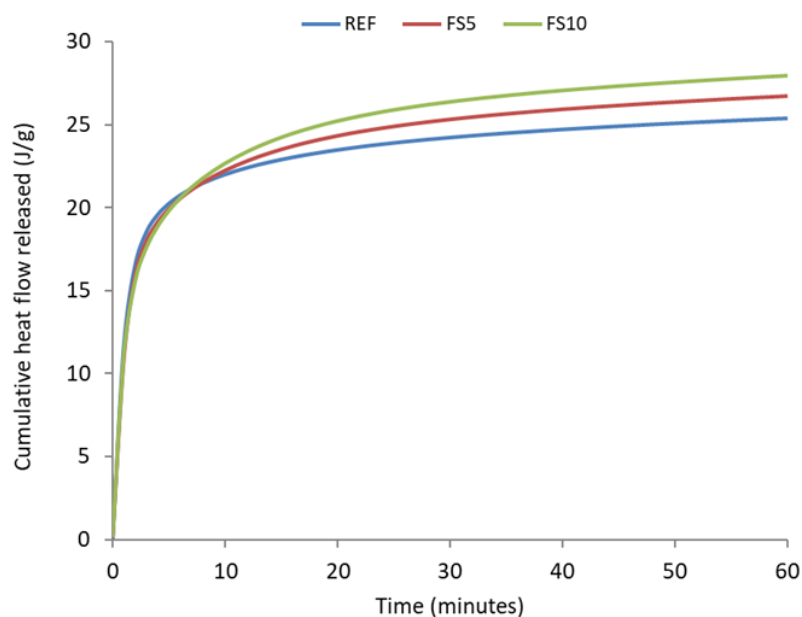


Figure 15. Cumulative heat release of REF, FS5, and FS10 during the first 60 min.

4. Conclusions

This paper aimed to recycle thermally treated flash-calcined dredged sediment in the development of an eco-friendly 3D-printable mortar, to reduce the usage of cement as well as the environmental impact and CO₂ emissions resulting from cement manufacturing. Mixtures with different percentages of flash-calcined sediment (0, 5, 10, 15, 20, and 30%) were characterized in their fresh and hardened states to test their adaptability for 3D printing. The main findings of this study are the following:

- The extrudability test using a manual gun device showed that it was possible to extrude mixtures with up to 10% of flash-calcined sediment. Mixtures containing 15% and 20% of flash-calcined sediment were very hard to extrude, whereas the mixture containing 30% of flash-calcined sediment was very dry and nonextrudable, and therefore was abandoned for the rest of the study.
- The buildability test using the modified minislump setup showed that all mixtures were buildable and had good shape-retention ability.
- Mixtures with 5% and 10% of flash-calcined sediment were printable using a 2 cm diameter nozzle (extrudable and buildable); however, those containing 15% and 20% of flash-calcined sediment were nonprintable (nonextrudable but buildable).
- The printability of the mixture containing 10% of flash-calcined sediment was confirmed by printing on a larger scale using a three-axis gantry printer.
- The addition of flash-calcined sediment decreased the flowability and shortened the setting time of mortars.
- The fall cone test showed that the evolution of the yield stress and the structural buildup of the tested mortars was linear with time and that the addition of flash-calcined sediment led to a faster structural buildup of mortars.
- Nonprinted samples with 5% and 10% of flash-calcined sediment showed a similar to higher compressive strength compared to that of the reference mortar, whereas a slightly lower compressive strength was recorded for mortars with a higher cement substitution by flash-calcined sediment (15% and 20%).
- Printed samples recorded an equal to lower compressive strength than that of non-printed samples, due to a larger porosity associated with the placement technique, as printed samples were laid down layer by layer without any compaction, whereas non-printed samples were compacted during placement, eliminating the higher porosity.

- Isothermal calorimetry showed that tested cement pastes with and without flash-calcined sediment presented similar calorimetric curves with identical phases. The addition of flash-calcined sediment did not majorly affect the hydration process of the pastes. However, the cumulative heat of hydration within the first hour showed that FS10 had the shortest setting time, followed by FS5, then REF, which complied with the results obtained by the Vicat test.

Because of the wide variety of sediment origins, types, and complex compositions and the demanding criteria and requirements of 3D printing, it is critical to expand this research to look into the effects of adding other types of sediments in cementitious 3D-printing applications. It would also be interesting to study the long-term durability of the developed waste-based mortars and to maximize the percentage of flash-calcined sediment addition.

Furthermore, based on the findings of this study, it would be interesting to explore the benefits of the fineness of flash-calcined sediment as well as the stiffness and viscosity it generates when added to printable cementitious materials, giving it a role of a natural viscosity-modifying agent. If that can be proven in future work, the recycling of flash-calcined sediment in 3D printing would therefore not only help reduce the environmental impact by decreasing cement consumption but also help minimize the usage of admixtures that are commonly required to ensure adequate viscosity of printable mixtures.

Author Contributions: Funding acquisition, N.-E.A.; investigation, J.D.; methodology, J.K., M.B. and G.A.; project administration, N.-E.A.; resources, M.B., N.-E.A. and G.A.; supervision, J.K., M.B., N.-E.A. and G.A.; validation, M.B., N.-E.A. and G.A.; visualization, J.D. and J.K.; writing—original draft, J.D.; writing—review and editing, J.K., M.B., N.-E.A. and G.A. All authors have read and agreed to the published version of the manuscript.

Funding: This research was funded by Chaire Industrielle ECOSED and the APC was funded by Chaire Industrielle ECOSED.

Institutional Review Board Statement: Not applicable.

Informed Consent Statement: Not applicable.

Data Availability Statement: The data presented in this study are available on request from the corresponding author.

Acknowledgments: The authors sincerely acknowledge the Chaire Industrielle ECOSED for funding this research work.

Conflicts of Interest: The authors declare no conflict of interest.

References

1. Zhao, Z.; Benzerzour, M.; Abriak, N.E.; Damidot, D.; Courard, L.; Wang, D. Use of uncontaminated marine sediments in mortar and concrete by partial substitution of cement. *Cem. Concr. Compos.* **2018**, *93*, 155–162. [[CrossRef](#)]
2. Dubois, V.; Abriak, N.E.; Zentar, R.; Ballivy, G. The use of marine sediments as a pavement base material. *Waste Manag.* **2009**, *29*, 774–782. [[CrossRef](#)] [[PubMed](#)]
3. Cappuyns, V.; Deweirt, V.; Rousseau, S. Dredged sediments as a resource for brick production: Possibilities and barriers from a consumers' perspective. *Waste Manag.* **2015**, *38*, 372–380. [[CrossRef](#)]
4. Lafhaj, Z.; Samara, M.; Agostini, F.; Boucard, L.; Skoczylas, F.; Depelseñaire, G. Polluted river sediments from the North region of France: Treatment with Novosol[®] process and valorization in clay bricks. *Constr. Build. Mater.* **2008**, *22*, 755–762. [[CrossRef](#)]
5. Hamer, K.; Karius, V. Brick production with dredged harbour sediments. An industrial-scale experiment. *Waste Manag.* **2002**, *22*, 521–530. [[CrossRef](#)]
6. Samara, M.; Lafhaj, Z.; Chapiseau, C. Valorization of stabilized river sediments in fired clay bricks: Factory scale experiment. *J. Hazard. Mater.* **2009**, *163*, 701–710. [[CrossRef](#)]
7. Dalton, J.L.; Gardner, K.H.; Seager, T.P.; Weimer, M.L.; Spear, J.C.M.; Magee, B.J. Properties of Portland cement made from contaminated sediments. *Resour. Conserv. Recycl.* **2004**, *41*, 227–241. [[CrossRef](#)]
8. Junakova, N.; Junak, J. Recycling of Reservoir Sediment Material as a Binder in Concrete. *Procedia Eng.* **2017**, *180*, 1292–1297. [[CrossRef](#)]
9. Amar, M.; Benzerzour, M.; Kleib, J.; Abriak, N.E. From dredged sediment to supplementary cementitious material: Characterization, treatment, and reuse. *Int. J. Sediment Res.* **2020**, *36*, 92–109. [[CrossRef](#)]

10. Benzerzour, M.; Maherzi, W.; Amar, M.A.A.; Abriak, N.E.; Damidot, D. Formulation of mortars based on thermally treated sediments. *J. Mater. Cycles Waste Manag.* **2018**, *20*, 592–603.
11. Aouad, G.; Laboudigue, A.; Gineys, N.; Abriak, N.E. Dredged sediments used as novel supply of raw material to produce Portland cement clinker. *Cem. Concr. Compos.* **2012**, *34*, 788–793. [[CrossRef](#)]
12. Chu, D.C.; Kleib, J.; Amar, M.; Benzerzour, M.; Abriak, N.E. Recycling of dredged sediment as a raw material for the manufacture of Portland cement—Numerical modeling of the hydration of synthesized cement using the CEMHYD3D code. *J. Build. Eng.* **2022**, *48*, 103871. [[CrossRef](#)]
13. Scrivener, K.L.; John, V.M.; Gartner, E.M. Eco-efficient cements: Potential economically viable solutions for a low-CO₂ cement-based materials industry. *Cem. Concr. Res.* **2018**, *114*, 2–26. [[CrossRef](#)]
14. Salvador, S.; Pons, O. Semi-mobile flash dryer/calciner unit to manufacture pozzolana from raw clay soils-application to soil stabilisation. *Constr. Build. Mater.* **2000**, *14*, 109–117. [[CrossRef](#)]
15. Snellings, R.; Horckmans, L.; Van Bunderen, C.; Vandewalle, L.; Cizer, Ö. Flash-calcined dredging sediment blended cements: Effect on cement hydration and properties. *Mater. Struct. Constr.* **2017**, *50*, 241. [[CrossRef](#)]
16. ASTM. International F2792-12a-Standard Terminology for Additive Manufacturing Technologies. *Rapid Manuf. Assoc.* **2013**, 10–12. [[CrossRef](#)]
17. Nematollahi, B.; Xia, M.; Sanjayan, J. Current progress of 3D concrete printing technologies. In Proceedings of the ISARC 2017—34th International Symposium on Automation and Robotics in Construction, Taipei, Taiwan, 28 June–1 July 2017; pp. 260–267.
18. Allen, S.M.; Sachs, E.M. Three-dimensional printing of metal parts for tooling and other applications. *Met. Mater. Int.* **2000**, *6*, 589–594. [[CrossRef](#)]
19. Pelz, J.S.; Ku, N.; Meyers, M.A.; Vargas-Gonzalez, L.R. Additive manufacturing of structural ceramics: A historical perspective. *J. Mater. Res. Technol.* **2021**, *15*, 670–695. [[CrossRef](#)]
20. Jafferson, J.M.; Chatterjee, D. A review on polymeric materials in additive manufacturing. *Mater. Today Proc.* **2021**, *46*, 1349–1365. [[CrossRef](#)]
21. Singamneni, S.; LV, Y.; Hewitt, A.; Chalk, R.; Thomas, W.; Jordison, D. Additive Manufacturing for the Aircraft Industry: A Review. *J. Aeronaut. Aerosp. Eng.* **2019**, *8*, 1–13. [[CrossRef](#)]
22. Culmone, C.; Smit, G.; Breedveld, P. Additive manufacturing of medical instruments: A state-of-the-art review. *Addit. Manuf.* **2019**, *27*, 461–473. [[CrossRef](#)]
23. Mantihal, S.; Kobun, R.; Lee, B.B. 3D food printing of as the new way of preparing food: A review. *Int. J. Gastron. Food Sci.* **2020**, *22*, 100260. [[CrossRef](#)]
24. Pegna, J. Exploratory investigation of solid freeform construction. *Autom. Constr.* **1997**, *5*, 427–437. [[CrossRef](#)]
25. Khoshnevis, B. Automated construction by contour crafting-Related robotics and information technologies. *Autom. Constr.* **2004**, *13*, 5–19. [[CrossRef](#)]
26. Cesaretti, G.; Dini, E.; De Kestelier, X.; Colla, V.; Pambaguian, L. Building components for an outpost on the Lunar soil by means of a novel 3D printing technology. *Acta Astronaut.* **2014**, *93*, 430–450. [[CrossRef](#)]
27. Lim, S.; Buswell, R.A.; Le, T.T.; Austin, S.A.; Gibb, A.G.F.; Thorpe, T. Developments in construction-scale additive manufacturing processes. *Autom. Constr.* **2012**, *21*, 262–268. [[CrossRef](#)]
28. Lim, S.; Le, T.; Webster, J.; Buswell, R.; Austin, S.; Gibb, A.; Thorpe, T. Fabricating construction components using layer manufacturing technology. *Proc. Int. Conf. Glob. Innov. Constr.* **2009**, 512–520.
29. Le, T.T.; Austin, S.A.; Lim, S.; Buswell, R.A.; Gibb, A.G.F.; Thorpe, T. Mix design and fresh properties for high-performance printing concrete. *Mater. Struct. Constr.* **2012**, *45*, 1221–1232. [[CrossRef](#)]
30. Tay, Y.W.; Panda, B.; Paul, S.C.; Tan, M.J.; Qian, S.Z.; Leong, K.F.; Chua, C.K. Processing and properties of construction materials for 3D printing. *Mater. Sci. Forum* **2016**, *861*, 177–181. [[CrossRef](#)]
31. Perrot, A.; Rangeard, D.; Pierre, A. Structural built-up of cement-based materials used for 3D-printing extrusion techniques. *Mater. Struct. Constr.* **2016**, *49*, 1213–1220. [[CrossRef](#)]
32. Batikha, M.; Jotangia, R.; Baaj, M.Y.; Mousleh, I. 3D concrete printing for sustainable and economical construction: A comparative study. *Autom. Constr.* **2022**, *134*, 104087. [[CrossRef](#)]
33. Klyuev, S.; Klyuev, A.; Fediuk, R.; Ageeva, M.; Fomina, E.; Amran, M.; Murali, G. Fresh and mechanical properties of low-cement mortars for 3D printing. *Constr. Build. Mater.* **2022**, *338*, 127644. [[CrossRef](#)]
34. Ma, G.; Li, Z.; Wang, L. Printable properties of cementitious material containing copper tailings for extrusion based 3D printing. *Constr. Build. Mater.* **2018**, *162*, 613–627. [[CrossRef](#)]
35. Kazemian, A.; Yuan, X.; Cochran, E.; Khoshnevis, B. Cementitious materials for construction-scale 3D printing: Laboratory testing of fresh printing mixture. *Constr. Build. Mater.* **2017**, *145*, 639–647. [[CrossRef](#)]
36. Chen, Y.; Romero Rodriguez, C.; Li, Z.; Chen, B.; Çopuroğlu, O.; Schlangen, E. Effect of different grade levels of calcined clays on fresh and hardened properties of ternary-blended cementitious materials for 3D printing. *Cem. Concr. Compos.* **2020**, *114*, 103708. [[CrossRef](#)]
37. Panda, B.; Ruan, S.; Unluer, C.; Tan, M.J. Improving the 3D printability of high volume fly ash mixtures via the use of nano attapulgite clay. *Compos. Part B Eng.* **2019**, *165*, 75–83. [[CrossRef](#)]

38. Kaushik, S.; Sonebi, M.; Amato, G.; Perrot, A.; Das, U.K. Influence of nanoclay on the fresh and rheological behaviour of 3D printing mortar. *Mater. Today Proc.* **2022**, *58*, 1063–1068. [[CrossRef](#)]
39. Bhattacharjee, S.; Basavaraj, A.S.; Rahul, A.V.; Santhanam, M.; Gettu, R.; Panda, B.; Schlangen, E.; Chen, Y.; Copuroglu, O.; Ma, G.; et al. Sustainable materials for 3D concrete printing. *Cem. Concr. Compos.* **2021**, *122*, 104156. [[CrossRef](#)]
40. Dey, D.; Srinivas, D.; Panda, B.; Suraneni, P.; Sitharam, T.G. Use of industrial waste materials for 3D printing of sustainable concrete: A review. *J. Clean. Prod.* **2022**, *340*, 130749. [[CrossRef](#)]
41. Rehman, A.U.; Lee, S.M.; Kim, J.H. Use of municipal solid waste incineration ash in 3D printable concrete. *Process Saf. Environ. Prot.* **2020**, *142*, 219–228. [[CrossRef](#)]
42. Ilcan, H.; Sahin, O.; Kul, A.; Yildirim, G.; Sahmaran, M. Rheological properties and compressive strength of construction and demolition waste-based geopolymer mortars for 3D-Printing. *Constr. Build. Mater.* **2022**, *328*, 127114. [[CrossRef](#)]
43. Ding, T.; Xiao, J.; Qin, F.; Duan, Z. Mechanical behavior of 3D printed mortar with recycled sand at early ages. *Constr. Build. Mater.* **2020**, *248*, 118654. [[CrossRef](#)]
44. Khalil, N.; Aouad, G.; El Cheikh, K.; Rémond, S. Use of calcium sulfoaluminate cements for setting control of 3D-printing mortars. *Constr. Build. Mater.* **2017**, *157*, 382–391. [[CrossRef](#)]
45. Baz, B.; Aouad, G.; Kleib, J.; Bulteel, D.; Remond, S. Durability assessment and microstructural analysis of 3D printed concrete exposed to sulfuric acid environments. *Constr. Build. Mater.* **2021**, *290*, 123220. [[CrossRef](#)]
46. Nematollahi, B.; Xia, M.; Sanjayan, J.; Vijay, P. Effect of type of fiber on inter-layer bond and flexural strengths of extrusion-based 3D printed geopolymer. *Mater. Sci. Forum* **2018**, *939*, 155–162. [[CrossRef](#)]
47. Baz, B.; Remond, S.; Aouad, G. Influence of the mix composition on the thixotropy of 3D printable mortars. *Mag. Concr. Res.* **2022**, *74*, 271–283. [[CrossRef](#)]
48. Estellé, P.; Michon, C.; Lanos, C.; Grossiord, J.L. Chapitre 7: De l'intérêt d'une caractérisation rhéologique empirique et relative. *La Mes. En Rhéologie* **2021**, 205–248. [[CrossRef](#)]
49. Kleib, J.; Aouad, G.; Khalil, N.; Zakhour, M. Incorporation of zinc in calcium sulfoaluminate cement clinker. *Adv. Cem. Res.* **2021**, *33*, 311–317. [[CrossRef](#)]
50. Kleib, J.; Aouad, G.; Abriak, N.E.; Benzerzour, M. Production of Portland cement clinker from French Municipal Solid Waste Incineration Bottom Ash. *Case Stud. Constr. Mater.* **2021**, *15*, e00629. [[CrossRef](#)]
51. Brooks, J.J.; Megat Johari, M.A.; Mazloom, M. Effect of admixtures on the setting times of high-strength concrete. *Cem. Concr. Compos.* **2000**, *22*, 293–301. [[CrossRef](#)]
52. Lu, B.; Weng, Y.; Li, M.; Qian, Y.; Leong, K.F.; Tan, M.J.; Qian, S. A systematical review of 3D printable cementitious materials. *Constr. Build. Mater.* **2019**, *207*, 477–490. [[CrossRef](#)]
53. Roussel, N. Steady and transient flow behaviour of fresh cement pastes. *Cem. Concr. Res.* **2005**, *35*, 1656–1664. [[CrossRef](#)]
54. Roussel, N. A thixotropy model for fresh fluid concretes: Theory, validation and applications. *Cem. Concr. Res.* **2006**, *36*, 1797–1806. [[CrossRef](#)]
55. Lootens, D.; Jousset, P.; Martinie, L.; Roussel, N.; Flatt, R.J. Yield stress during setting of cement pastes from penetration tests. *Cem. Concr. Res.* **2009**, *39*, 401–408. [[CrossRef](#)]
56. Rahul, A.V.; Santhanam, M.; Meena, H.; Ghani, Z. 3D printable concrete: Mixture design and test methods. *Cem. Concr. Compos.* **2019**, *97*, 13–23. [[CrossRef](#)]
57. Amar, M.A.A. Traitement des Sédiment de Dragage Pour une Valorisation dans les Matrice Cimentaires. Ph.D. Thesis, University of Lille 1, Lille, France, 2017.
58. Le, T.T.; Austin, S.A.; Lim, S.; Buswell, R.A.; Law, R.; Gibb, A.G.F.; Thorpe, T. Hardened properties of high-performance printing concrete. *Cem. Concr. Res.* **2012**, *42*, 558–566. [[CrossRef](#)]
59. Panda, B.; Paul, S.C.; Hui, L.J.; Tay, Y.W.D.; Tan, M.J. Additive manufacturing of geopolymer for sustainable built environment. *J. Clean. Prod.* **2017**, *167*, 281–288. [[CrossRef](#)]
60. Jansen, D.; Goetz-Neunhoeffer, F.; Stabler, C.; Neubauer, J. A remastered external standard method applied to the quantification of early OPC hydration. *Cem. Concr. Res.* **2011**, *41*, 602–608. [[CrossRef](#)]
61. Fierens, P.; Verhaegen, J.P. Hydration of tricalcium silicate in paste-Kinetics of calcium ions dissolution in the aqueous phase. *Cem. Concr. Res.* **1976**, *6*, 337–342. [[CrossRef](#)]
62. Tennis, P.D.; Jennings, H.M. Model for two types of calcium silicate hydrate in the microstructure of Portland cement pastes. *Cem. Concr. Res.* **2000**, *30*, 855–863. [[CrossRef](#)]